

Quantum Monte Carlo study of the one-dimensional ionic Hubbard model

Tim Wilkens and Richard M. Martin

Department of Physics and Materials Research Laboratory, University of Illinois, Urbana, Illinois 61801

(Received 23 June 2000; revised manuscript received 10 January 2001; published 16 May 2001)

Quantum Monte Carlo methods are used to study a quantum phase transition in a one-dimensional Hubbard model with on-site interaction U and a staggered ionic potential (Δ). Using recently formulated methods, the electronic polarization and localization are determined directly from the correlated ground state wave function and compared to results of previous work using exact diagonalization and Hartree-Fock. We find a transition from a symmetric band insulator to a broken-symmetry bond ordered (BO) phase as the ratio of U/Δ is increased, with a metallic point at the transition. Since it is known that at $\Delta=0$ the usual Hubbard model is a Mott insulator (MI) with no long-range order, we have searched for a second transition to this state by (i) increasing U at fixed Δ and (ii) decreasing Δ at fixed U . We find no transition from the BO to MI state, and we propose that the symmetric MI state exists only at $\Delta=0$.

DOI: 10.1103/PhysRevB.63.235108

PACS number(s): 71.27.+a, 71.30.+h, 77.90.+k, 77.65.-j

I. INTRODUCTION

Strongly correlated systems of interacting electrons lead to many of the most interesting phenomena observed in solid state physics.¹ As a function of the interaction strength, there can be quantum phase transitions¹ characterized by an order parameter with the possible development of long-range order and a transition to a broken symmetry state. Interactions can also lead to “Mott insulators” (MI) and to metal-insulator transitions.² An important question is whether or not in the thermodynamic limit a Mott insulator must be associated with a phase transition that is accompanied by a broken symmetry and a corresponding order parameter. In his original work, Mott³ argued that the insulating character did not depend upon an order parameter. On the other hand, Slater⁴ emphasized the relation of the insulating behavior to the long range order, and in many cases it is known that the MI state must be accompanied by a broken symmetry.⁵

To address such issues theoretically we must have methods that can clearly distinguish metals from insulators, i.e., the ability to transport charge⁶⁻⁸ vs localization of the electrons.⁸ Insulators at absolute zero cannot transport arbitrary amounts of charge macroscopic distances across their bulk; however, the center of electronic charge can shift in response to external fields, which is described in terms of changes in polarization.^{6,7} The polarizability is characterized by the degree of electronic delocalization⁸ which increases with the proximity to the metallic state. Recently, there have been new developments defining macroscopic polarization and localization in terms of the insulating ground state wave function.⁹⁻¹⁵ These theories formulate the polarization and localization in terms of Berry’s phases¹⁶ which can be calculated using “twisted boundary conditions” or in terms of the expectation value of an exponentiated operator. Such twisted boundary conditions have been applied in the past to study metals and approach metal-insulator transitions from the metallic side.^{17-19,8} With the recently developed methods for insulators, there are now complementary tools¹⁵ to provide quantitative information on the divergence of the localization length as one approaches the metal-insulator transition from the insulating side.

Generalized Hubbard models^{20,21} are well suited for studies of fundamental issues regarding metals and insulators because they are simple models that exhibit a wide range of behaviors depending upon the parameters in the models. The simplest of all, the original Hubbard model with an on-site interaction U and nearest neighbor hopping t in one dimension (1D), was solved exactly by Lieb and Wu.²² Their paper conveys the point that there is no change of spatial symmetry and no phase transition at any positive U . At half-filling the model is metallic at $U=0$, whereas for $U>0$ a gap exists to charge excitations but no gap exists to spin excitations. This is commonly referred to as the MI state, but in this case there is no “Mott transition.” At any other filling, the model is always metallic. There is never a state that would be called an ordinary band insulating (BI) state. However, in systems of higher dimensionality ($d \geq 2$), a MI state is always accompanied by a broken symmetry.⁵

Many new possibilities emerge for generalized Hubbard models in 1D. In this paper we study the half-filled ionic 1D Hubbard model with two inequivalent sites, proposed by Nagaosa²³ and later by Egami²⁴ as a model ferroelectric. Since there are two electrons per cell, one expects a transition to occur from an ionic band insulator to a strongly correlated Mott insulator as U is increased. Evidence for such a transition was found in exact-diagonalization calculations,^{13,10} where the electronic polarization was found to jump abruptly between two discrete values fixed by the existence of two centers of inversion at the two sites. Such behavior has been termed a “topological transition.”¹⁴ These calculations find that the model has a metallic point separating two symmetric insulating phases and that a ferroelectric polarization results only if the atomic sites are displaced from the centers of inversion.

However, recently Fabrizio *et al.*²⁵ have proposed that this model will instead exhibit two quantum phase transitions: one from a BI state to a long range bond ordered (BO) state, predicted to be in the Ising universality class, and a second from the BO to the MI state, predicted to be a Kosterlitz-Thouless transition. Such transitions to BO states have recently been found in 1D Hubbard models with extended interactions ($U-V$) by Nakamura.^{26,27} The BO state

is a broken symmetry state in which the system becomes ferroelectric due strictly to electron-electron interactions even if all the atoms are at centers of inversion.

During the course of the present work, two preprints have reported calculations of charge and spin gaps in the model.^{28,29} Even though each work uses the density matrix renormalization group (DRMG) that allows studies of very large 1D systems, each group reports great difficulty in extrapolating to large size the small spin gaps and the two papers come to opposite conclusions regarding the existence of the BO state.

The purpose of this paper is to study the half-filled ionic Hubbard model using a method that (i) will treat electron correlation exactly and (ii) scale to large systems needed near second-order phase transitions. For these reasons we use quantum Monte Carlo³⁰(QMC) which in principle is exact since there is no ‘‘fermion sign problem’’ because electrons of the same spin never exchange in this model. This is due to the fact that there is only nearest-neighbor hopping and there cannot be two electrons of the same spin on any site. The only qualifications to this statement in our methods are that there must be nonzero overlap between our trial function and the true ground state, and the simulation must be capable of reaching the ground state in practice.

To our knowledge this is the first QMC study of polarization and localization in any system. Of course, Monte Carlo simulations have been widely employed in studying metal-insulator transitions and localization (see, for example, Refs. 23,31–33). The application here is to study *both polarization and localization*. In particular, the present work is the first study of the ionic Hubbard model with systems large enough to determine quantitatively the nature of the transitions and whether or not there exists the spontaneously bond-ordered phase proposed by Fabrizio *et al.*²⁵ Furthermore, if there are indeed quantum phase transitions in the ionic model—whereas it is known that there are none in the usual nonionic Hubbard model—then it follows that one must address the issue: Is a critical degree of ionicity required, or is the usual Hubbard model unstable to infinitesimal ionic perturbations? It is known^{34–37,33} that the usual Hubbard model is unstable to dimerization at all U . Thus a second question is does this instability play a fundamental role in stabilizing the bond-ordered state?

The organization of the paper is as follows. In Sec. II, we introduce the model studied in this paper. In certain cases, depending upon the parameters of the Hamiltonian, this model is exactly soluble. We discuss the relevance of these solutions to the more general case studied in this paper. In Sec. III formulas for evaluating the electronic polarization and localization are presented. In Sec. IV, we introduce the quantum Monte Carlo (QMC) methods employed to evaluate expectation values and we describe their respective limitations. These are variational and Green’s function Monte Carlo algorithms and the ‘‘forward walking’’ method for computing expectation values of operators that do not commute with the Hamiltonian. Our results are presented in Sec. V and comparisons are made with previous studies using exact diagonalization and Hartree-Fock. In Sec. VI, we discuss the differences between our results and previous studies

and the consequences of our new findings.

II. THE MODEL

The generalized ionic Hubbard Hamiltonian²³ is defined by

$$\hat{H} = \hat{H}_0(t_0, U) + \hat{H}_{\text{ion}}(\Delta) + \hat{H}_{\text{dim}}(x), \quad (1)$$

where \hat{H}_0 is the Hamiltonian of the usual Hubbard model

$$\hat{H}_0(t_0, U) = \sum_{i,\sigma} t_0 (c_{i+1,\sigma}^\dagger c_{i,\sigma} + c_{i,\sigma}^\dagger c_{i+1,\sigma}) + U \sum_{i=1}^L \hat{n}_{i,\sigma} \hat{n}_{i,-\sigma}. \quad (2)$$

Here $c_{i,\sigma}^\dagger (c_{i,\sigma})$ creates (destroys) an electron of spin σ on site s while $\hat{n}_{i,\sigma} = c_{i,\sigma}^\dagger c_{i,\sigma}$ is the density operator of electrons of spin σ on site i . The ionic term

$$\hat{H}_{\text{ion}}(\Delta) = \Delta \sum_{i,\sigma} (-1)^i \hat{n}_{i,\sigma}, \quad (3)$$

consists of an on-site energy ($\pm \Delta$) that alternates between neighboring sites, which is intended to model the electrostatic potential of cations and anions in an ionic material. Although dimerization, *per se* is not a primary objective of the present work, it is crucial to include a dimer term that breaks the inversion symmetry and is defined with the Su-Schrieffer-Heeger form³⁸

$$\hat{H}_{\text{dim}}(x) = t_0 \delta \hat{B}. \quad (4)$$

Here $\delta = \alpha x$ denotes a dimerization term in the Hamiltonian $\{t_i = t_0[1 + (-1)^i \delta]\}$ that incorporates the effect of alternately displacing the atoms $\pm x$ from their equilibrium positions $[R(i)_0 = ia]$ and α is the linear electron phonon coupling constant. The operator \hat{B} is the ‘‘bond order’’ operator

$$\hat{B} = \sum_i (-1)^i \hat{B}_i; \quad \hat{B}_i = \sum_{\sigma} (c_{i+1,\sigma}^\dagger c_{i,\sigma} + c_{i,\sigma}^\dagger c_{i+1,\sigma}), \quad (5)$$

which is a sum of staggered hopping operators. We can define average values per cell, e.g.,

$$B = \frac{2}{N} \langle \hat{B} \rangle, \quad (6)$$

were N is the number of sites and $N/2$, the number of cells. (Fabrizio *et al.* refer to this as a ‘‘dimerization’’ operator; however, we will use the term ‘‘bond order,’’²⁶ since it denotes a property of the electronic state and there may be a nonzero expectation value of the bond order $\langle \hat{B} \rangle$ even if the lattice is not dimerized.)

Exact analytic solutions for Eq. (1) exist in several limiting cases. In the noninteracting case ($U=0$), the electrons fill the lowest energy band $[E(k)]$

$$E(k) = \pm \{\Delta^2 + 4t_0^2 [\cos^2(k) + 4\delta^2 \sin^2(k)]\}^{1/2} \quad (7)$$

from $k = 0$ to $\pm \pi/2a$. In the case $\Delta = x = 0$ there is no gap at the Fermi surface and the system is metallic, but for any finite Δ or x a gap is opened at the Fermi surface and the system is a band insulator. If $\Delta = 0$ and we perturb the system by adjusting $x \neq 0$ the lattice is known to suffer the famous Peierls instability^{39,40} and energetically favors dimerization.

Exact solutions in the presence of correlation ($U \neq 0$) are restricted to cases in which (i) there is no intersite coupling ($t = 0$), (ii) there is a large displacement such that $\delta = 1$ and the lattice is completely deformed into an array of independent dimers, or (iii) the case of the usual Hubbard model where there is no ionic potential or lattice deformation ($\Delta = \delta = 0$) for which there are exact analytic solutions²² for all U . In the last case, the exact solution predicts that at half-filling the system becomes a Mott insulator for any nonzero U . There is no change of symmetry from the case of $U = 0$ and in the limit of large U/t_0 the system reduces to the Heisenberg spin model, with nearest-neighbor exchange $J = 4t^2 U / (U^2 - 4\Delta^2)$, which also has no long range order or spin gap in one dimension. The MI and BI regimes are commonly distinguished from one another in literature on the basis of spin-charge separation.⁴¹ In both cases there is a gap to charge excitations but in the MI state the spin gap is zero while in the BI state both spin and charge gaps are nonzero.

The limiting cases (i) and (ii) are also instructive for our purposes. In the former ($t_0 = 0$) there is a transition at $\Delta = U$ from a singlet state with two electrons on the site with on site energy $-\Delta$, which is similar to a band insulator, to a state with one electron per site which has a spin on each site and is similar to a Mott insulator. Thus one might expect a transition from the BI state to some other phase as U is increased even if $t_0 \neq 0$. The second case (ii) with $\delta = 1$ and $t_0 \neq 0$ always leads to a singlet ground state for the isolated dimers,⁴³ which relates to the known result that one has a singlet state with a gap for both spin and charge excitations for any degree of dimerization. Thus one can ask: does a transition occur from the BI to MI regime as $\delta \rightarrow 0$ for $U \neq 0$? Is there a spontaneous²⁵ bond-ordered phase? We shall test these ideas with our QMC simulations applied to the general case where there are no exact analytic solutions.

III. ELECTRONIC POLARIZATION AND LOCALIZATION

The issues associated with calculating the electric polarization in an extended system have a long, torturous history.^{42,44} Only recently have formulas been devised that express the polarization and localization of electrons directly in terms of the ground state wave function.^{9,10,44} One type of formulation measures the change in polarization as a Berry's phase obtained by integrating over twisted boundary conditions and an adiabatic parameter that characterizes the evolution of the system as it moves from one state to another.^{9,10} This approach has also been extended to localization in an independent particle formulation⁴⁵ and recently in a many-body formalism.¹⁵ An alternative approach has been developed by Resta and Sorella^{11,12} and others,^{14,15} who expressed the electronic polarization and localization in one dimension

in terms of the expectation value of a complex operator

$$\langle \hat{Z} \rangle = \left\langle e^{i(2\pi/L) \sum_i x_i} \right\rangle = \left\langle \prod_j e^{i(2\pi/L)x_j} \right\rangle, \quad (8)$$

where the average is taken with respect to a truly correlated many body wave function utilizing periodic boundary conditions (PBC) sampled using one of the quantum Monte Carlo techniques discussed in Sec. IV.

In terms of $\langle \hat{Z} \rangle$ the polarization of the many body ground state can be expressed as

$$\langle \Delta P_{el} \rangle = \lim_{L \rightarrow \infty} \frac{e}{2\pi} \text{Im} \ln \langle \hat{Z} \rangle, \quad (9)$$

and a measure of the electronic delocalization is given by

$$\langle \Delta \hat{X}^2 \rangle = \lim_{L \rightarrow \infty} - \left(\frac{L}{2\pi} \right)^2 \ln |\langle \hat{Z} \rangle|^2. \quad (10)$$

These expressions are exact only in the limit of an infinitely large system, and in practice one measures each for increasingly larger supercells until convergence is met. Recently Souza *et al.*¹⁵ have shown that Eqs. (9) and (10) are in fact valid in a correlated many-body system and related this formulation to that using twisted boundary conditions. They also demonstrated that the formulas relate directly to measurable fluctuations of the polarization, thus validating the two formulas as direct measures of electronic polarization and delocalization.

For our work we use quantum Monte Carlo techniques to evaluate Eqs. (9) and (10) which involve expectation values of quantities using wavefunctions that satisfy periodic boundary conditions. This is a great advantage in QMC since we can use the same methods developed for other problems.³⁰ The alternative approach using twisted boundary conditions would require a change in the algorithms to use a ‘‘fixed phase’’^{46,47} rather than a fixed node method. Such an approach would have important advantages, in particular, it would allow calculations to be done on smaller supercells.¹⁵ In the present study, however, we need to work with large systems because of long correlation lengths near the phase transitions and thus it is convenient to use the standard methods.

IV. QUANTUM MONTE CARLO

Quantum Monte Carlo (QMC) methods^{48,30} make it possible to evaluate expectation values of operators in many-body systems by stochastically sampling a probability distribution. In this paper we focus on two methods, variational Monte Carlo (VMC) and Greens function Monte Carlo (GFMC), that can be used to determine properties at temperature equal zero. The space of integration is the set of all the electronic coordinates $\mathbf{R} \equiv \{\vec{r}_1, \dots, \vec{r}_N\}$, which is sampled by ‘‘walkers’’ which denote a set of configurations $\{\mathbf{R}\}$. A random walk is generated by starting from an initial configuration \mathbf{R}_0 , from which new configurations are generated by successively stepping to new random configurations,

e.g., using a generalized Metropolis method.⁴⁹ This is done by accepting or rejecting new configurations at each step based upon a chosen acceptance function $[P(\mathbf{R})]$. After a period of time the walk will stabilize such that the set of configurations visited $\{\mathbf{R}\}$ will be distributed according to $P(\mathbf{R})$.

A. Variational Monte Carlo

In VMC the expectation values are found for an arbitrary operator \hat{O} with a variational trial wave function $[\Psi_T(\{\alpha\}, \mathbf{R})]$, where $\{\alpha\}$ denotes a set of parameters that can be optimized. The expectation value can be written as a high-dimensional integral over coordinate positions \mathbf{R}

$$\begin{aligned} \langle \hat{O} \rangle_{\text{VMC}} &= \frac{\int \Psi_T(\{\alpha\}, \mathbf{R}) \hat{O} \Psi_T(\{\alpha\}, \mathbf{R}) d\mathbf{R}}{\int |\Psi_T(\{\alpha\}, \mathbf{R})|^2 d\mathbf{R}} \\ &= \frac{\int |\Psi_T(\{\alpha\}, \mathbf{R})|^2 \hat{O}_L(\mathbf{R}) d\mathbf{R}}{\int |\Psi_T(\{\alpha\}, \mathbf{R})|^2 d\mathbf{R}}, \end{aligned} \quad (11)$$

where $\hat{O}_L(\mathbf{R}) = \hat{O} \Psi_T(\mathbf{R}) / \Psi_T(\mathbf{R})$. The integral may be found by sampling a set of points ($\{\mathbf{R}\}$) distributed according to the modulus of the wave function, generated by the Metropolis algorithm with $|\Psi_T|^2$ as the acceptance function. VMC is easy to implement but is limited in accuracy by the form of the adopted wave function. In our work Ψ_T has the Gutzwiller form⁵⁰

$$\Psi_T(g, \Delta', \delta') = \underbrace{g^{\sum_{i=1}^L \hat{n}_{i\uparrow} \hat{n}_{i\downarrow}}}_{\text{Jastrow Term}} D_{\uparrow}(\Delta', \delta') D_{\downarrow}(\Delta', \delta'), \quad (12)$$

which is a product of Slater determinants for each spin (thus guaranteeing that the wave function is antisymmetric) and a two body Jastrow correlation function that reduces the amplitude of configurations with doubly occupied sites for $0 < g \leq 1$, thus lowering the interaction energy. The single body portion of Eq. (1) is parametrized by Δ' and δ' , which means the orbitals used to construct the Slater determinants are obtained by diagonalizing the noninteracting ($U=0$) portion of the Hamiltonian $[\hat{H}(\Delta', \delta')]$ and adjusting (Δ', δ') to optimal values that minimize the energy in Eq. (11) with respect to $\Psi_T(g, \Delta', \delta')$.

B. Green's function Monte Carlo (GFMC) for discrete systems

GFMC starts with the optimized VMC wave function $\Psi_T(g, \Delta', \delta')$ upon which a projection is applied to obtain an improved ground state. To illustrate the principles upon which this method depends, one can expand Ψ_T in terms of the eigenstates Ψ_i of \hat{H} . Then the imaginary time propagator acting upon Ψ_T has the form

$$e^{-\tau(\hat{H}-E_0)} \Psi_T = e^{-\tau(\hat{H}-E_0)} \sum_i C_i \Psi_i \rightarrow C_0 \Psi_0 \quad (13)$$

provided that τ is taken to be large. The following is a summary of the method developed by Haaf *et al.*⁵¹ some of which is used in the next section. For lattices this projection scheme takes advantage of the fact the spectrum of \hat{H} is bounded so that one can use a Green's function projection

$$e^{-\tau(\hat{H}-E_0)} \rightarrow [1 - \Delta \tau(\hat{H} - E_0)]^M |_{M\Delta\tau=\tau}. \quad (14)$$

The propagator acting upon the trial wavefunction now generates a series of functions

$$|\Psi^M\rangle = [1 - \Delta \tau(\hat{H} - E_0)]^M |\Psi_T\rangle. \quad (15)$$

In this algorithm there is no time step error⁵² so long as $|[1 - \Delta \tau(E_{\max} - E_0)]| < 1$, where E_{\max} is the maximum eigenvalue of the \hat{H} which is finite on a lattice. The exact ground state Ψ_0 is generated in the limit $M \rightarrow \infty$ so long as there is nonzero overlap between Ψ_0 and Ψ_T .

By inserting the identity operator $\sum_{\mathbf{R}} |\mathbf{R}\rangle \langle \mathbf{R}|$ between successive applications of the projection operator, the wavefunction at step M can be expressed as⁵¹

$$\Psi^M(\mathbf{R}_M) = \sum_{\mathbf{R}_{M-1}, \dots, \mathbf{R}_0} \Psi_T^{-1}(\mathbf{R}_M) \prod_{i=1}^M G(\mathbf{R}_i, \mathbf{R}_{i-1}) \Psi_T^2(\mathbf{R}_0). \quad (16)$$

The matrix elements of the Greens function between neighboring points in configuration space is

$$G(\mathbf{R}_i, \mathbf{R}_{i-1}) = \frac{\Psi_T(\mathbf{R}_i)}{\Psi_T(\mathbf{R}_{i-1})} \langle \mathbf{R}_i | [1 - \Delta \tau(\hat{H} - E_0)] | \mathbf{R}_{i-1} \rangle, \quad (17)$$

where the factor $\Psi_T(\mathbf{R}_i) / \Psi_T(\mathbf{R}_{i-1})$ introduces importance sampling.⁴⁸ Since the $G(\mathbf{R}_i, \mathbf{R}_{i-1})$ are not normalized to one, they cannot be interpreted directly as a probability distribution. This is remedied by expressing $G(\mathbf{R}_i, \mathbf{R}_{i-1})$ as

$$G(\mathbf{R}_i, \mathbf{R}_{i-1}) = m(\mathbf{R}_i, \mathbf{R}_{i-1}) p(\mathbf{R}_i, \mathbf{R}_{i-1}), \quad (18)$$

where $m(\mathbf{R}_i, \mathbf{R}_{i-1})$ is a weight defined so that p is normalized,⁵¹ $\sum_{\mathbf{R}_i} p(\mathbf{R}_i, \mathbf{R}_{i-1}) = 1$.

In the general case⁵¹ $m(\mathbf{R}_i, \mathbf{R}_{i-1})$ is not simply a weight but also includes the sign of $G(\mathbf{R}_i, \mathbf{R}_{i-1})$. This is the symptom of the sign problem that causes difficulties in Monte Carlo sampling since the weight of a walker must be positive definite if it is to be interpreted in a probabilistic manner. In general, one must make some approximation to remedy this problem, by fixing the sign of \mathbf{G} , e.g., the ‘‘fixed node approximation,’’ which has been described for lattice problems by ten Haff *et al.*⁵³ This is not a problem in the model considered here and is the reason why this model can be solved exactly by GFMC. In the present model the *only nodes* of the ground state wave function are the points where two electrons of the same spin cross, which are the same nodes as those of the trial wave function. The GFMC sampling is restricted to a region in which $G(\mathbf{R}_i, \mathbf{R}_{i-1})$ never changes sign because each step moves only one electron by one site,

with the move allowed only if the target site is not occupied by an electron of the same spin.

Implementation of the above method is as follows. A VMC calculation is performed which supplies a number of walkers $\{R\}$ initially distributed according to $|\Psi_T|^2$. Each of these are then randomly walked along a path in configuration space using $p(\mathbf{R}, \mathbf{R}')$ as the Metropolis acceptance function of moving from \mathbf{R} to \mathbf{R}' . Each step is weighted by $m(\mathbf{R}, \mathbf{R}')$ such that the i th walker's accumulated weight is

$$w_i^M = \prod_{i=1}^M m(\mathbf{R}_i, \mathbf{R}_{i-1}). \quad (19)$$

Expectation values for an arbitrary operator \hat{O} after M projections of the green's function are measured by averaging the weighted local form of $O_L(\mathbf{R})$ of each walker

$$\langle \hat{O} \rangle_{\text{GFMC}} = \frac{\langle \Psi_T | \hat{O} | \Psi^M \rangle}{\langle \Psi_T | \Psi^N \rangle} = \frac{\sum_i O_L(\mathbf{R}_M) w_i^M}{\sum_i w_i^M}. \quad (20)$$

Averages in GFMC equal the ground state expectation value only for those operators which commute with \hat{H} because the inner product Eq. (20) is a ‘‘mixed estimator’’ between $\langle \Psi_T |$ and $|\Psi_0\rangle$. Operators that commute with \hat{H} share the same eigenstates and the operator in Eq. (20) can be considered to act to right on Ψ_0 , thus returning the ground state and cancelling the normalization of the denominator. Conversely operators that do not commute with \hat{H} have different eigenstates and thus do not cancel the normalization of the denominator in Eq. (20). There are several ways to improve upon the GFMC mixed estimator for such expectation values. One is an approximation that is valid so long as the VMC and GFMC averages are close to one another. Expressing $|\Psi_0\rangle$ as $|\Psi_T\rangle + |\delta\Psi\rangle$ and taking the inner product, the ground state expectation value can be expressed as⁴⁸

$$\langle \Psi_0 | \hat{O} | \Psi_0 \rangle \approx 2 \langle \hat{O} \rangle_{\text{GFMC}} - \langle \hat{O} \rangle_{\text{VMC}} + O(\delta\Psi^2). \quad (21)$$

However, this approximation breaks down whenever the VMC trial wavefunction is not a good approximation to Ψ_0 .

C. Expectation values and forward walking

The exact ground state expectation value of any operator (\hat{O}) can be found if the mixed expression Eq. (20) is replaced by one involving the exact wave function in both the bra and ket

$$\frac{\langle \Psi_T | [1 - \Delta\tau(\hat{H} - E_0)]^{M'} \hat{O} [1 - \Delta\tau(\hat{H} - E_0)]^M | \Psi_T \rangle}{\langle \Psi_T | [1 - \Delta\tau(\hat{H} - E_0)]^{M'} [1 - \Delta\tau(\hat{H} - E_0)]^M | \Psi_T \rangle}. \quad (22)$$

This can be accomplished by ‘‘forward walking,’’⁴⁸ which can be simply expressed in terms of the GFMC method previously discussed. The same methods and terminology used in GFMC are also applicable here. Inserting the identity op-

erator between each projection and using importance sampling Eq. (22) can be rewritten as

$$\sum_{\mathbf{R}_{M+M'}, \dots, \mathbf{R}_1} \left[\prod_{i=M}^{M+M'-1} G(\mathbf{R}_{i+1}, \mathbf{R}_i) \right] O_L \times \left[\prod_{i=1}^{M-1} G(\mathbf{R}_{i+1}, \mathbf{R}_i) \right] \Psi_T^2(\mathbf{R}_0). \quad (23)$$

The $G(\mathbf{R}, \mathbf{R}')$ are sampled as before in terms of a probability function $[p(\mathbf{R}, \mathbf{R}')]$ and weight $[m(\mathbf{R}, \mathbf{R}')]$. A series of i walkers, initially distributed according to the VMC trial function, are stepped along paths ($\{\mathbf{R}_i\}$) in configuration space by Metropolis sampling. After N projections the accumulated weight of each $\{\mathbf{R}_i\}$ is the product of all steps weights, as defined in Eq. (19). The walkers weights are distributed according to the mixed probability distribution $\Psi_T(\mathbf{R}_M)\Psi_0(\mathbf{R}_M)$. The local form of \hat{O} [$O_i(\mathbf{R}_M)$] is measured for each walker but not averaged as it is in GFMC. The walkers are moved an additional M' steps in imaginary time over which they accumulate post measurement weights ($w_i^{M'}$). Averages are computed using each walkers accumulated weight before and after measuring $O_i(\mathbf{R}_M)$

$$\frac{\sum_i w_i^{M'} [w_i^M O_i(\mathbf{R}_M)]}{\sum_i w_i^{M'} w_i^M}. \quad (24)$$

Although this method is in principle exact, assuming the nodal structure of Ψ_0 is known, it also has its disadvantages. In particular, the width of the post-measurement weight distribution grows with the number of forward walking steps M' , thereby increasing the fluctuation of the forward walking estimates. To achieve the same statistical error as that in GFMC, forward walking may require many times more estimates in Eq. (24).

We have tested our algorithms using forward walking by calculating expectation values of operators that do not commute with the Hamiltonian, such as the bond order $\langle \hat{B} \rangle$ needed later. If we start from very poor trial functions, GFMC leads to energies that are independent of the trial function, but the approximate mixed estimator or the improved extrapolation do not. However, the forward walking expressions are exact within the numerical error estimates. For example, in a case where there is no broken symmetry the forward walking leads to the correct result $\langle \hat{B} \rangle = 0$ within the error estimates, even when the trial function is chosen to have large $\langle \hat{B} \rangle$.

D. Test of GFMC on ordinary Hubbard model

The accuracy with which the energy can be measured in GFMC and the magnitude of the finite size effects can be addressed by comparing with exact results for the usual Hubbard model at 1/2 filling, which have been evaluated by Hashimoto⁵⁴ for finite systems of $4N+2$ sites using periodic boundary conditions. In Fig. 1 the differences in energy be-

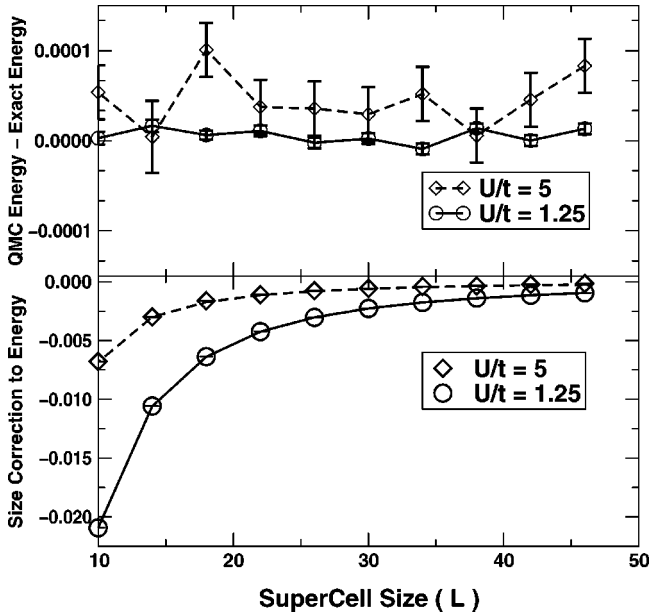


FIG. 1. In the lower figure $E(4N+2) - E(\infty)$ is plotted where $N=2,3,\dots,11$ and infinite system estimates are those of Lieb and Wu. The lines are exact results from Hashimoto (Ref. 54) and the symbols are the QMC estimates for (i) $U=5$ (diamonds) and (ii) $U=1.25$ (squares). In the top figure the energy difference between the QMC and exact results is plotted vs L .

tween lattices of size L and the thermodynamic limit is plotted for two cases $U/t_0=1.25,5.0$. The finite size effects at typical $U \approx 2.4$ are of order $0.0001 t_0$ for a supercell of 82 sites. Thus we do not anticipate any difficulty in calculating the energy except in cases where there is a much longer correlation length than in the usual Hubbard Model, e.g., near a phase transition where correlation lengths diverge.

For comparison to our work later it is useful also to study the dimerized Hubbard model with $\delta \neq 0$. Work on related issues in the past two decades has verified early theoretical predictions³⁴ that electron correlation enhances the Peierls instability of the noninteracting Hubbard model as $\delta \rightarrow 0$. Using the Hellman-Feynman theorem the bond order $\langle \hat{B} \rangle$ can be identified as the first derivative of the energy with respect to the lattice distortion αx or δ . The bond order susceptibility or the second derivative of the energy with respect to δ has a logarithmic divergence as $\delta \rightarrow 0$,⁴⁰ which is referred to as the Peierls instability. The energy near $\delta=0$ varies as⁵⁵

$$E(\delta=0) + A \delta^\gamma / \ln(\delta), \quad (25)$$

where the amplitude A and γ are dependent upon the strength of electron correlation. For $U=0$ A is proportional to t_0 and $\gamma=2$, and for $U/t_0 \ll 1$ variational methods suggest the same results. In the strongly correlated regime the lattice can be mapped onto a 1D Heisenberg lattice where A is proportional to $4t_0^2/U$ and $\gamma=4/3$. Although the instability is enhanced at large U , the effect is more difficult to observe since the electronic energy is much smaller.

In our studies we consider small ionic deviations ($\delta \neq 0$) from the usual Hubbard model for $U=2.4$. The QMC energy

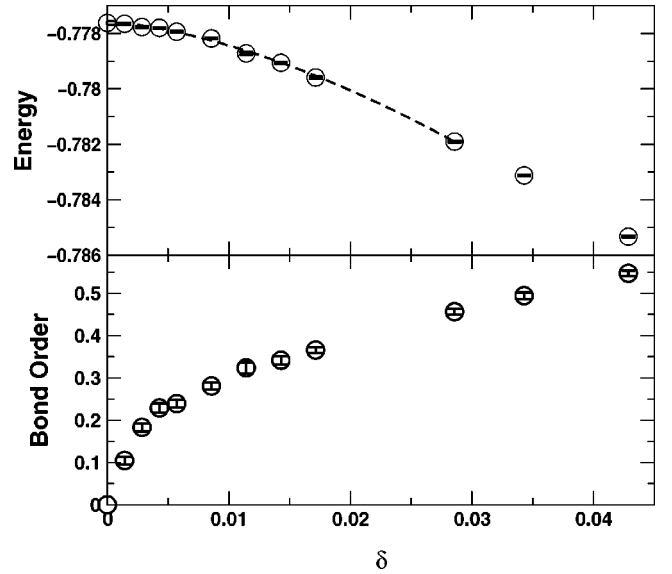


FIG. 2. Ground state energy and bond order vs lattice distortion δ for $U=2.4$ in the usual Hubbard model. The energy was fit to the function $E(\delta=0) + A \delta^\gamma / \ln(\delta)$ using a nonlinear least squares routine.

and bond order are plotted vs δ in Fig. 2 for an 82 site lattice. The GFMC energy was fit to Eq. 25 using a nonlinear least squares routine. The parameters of the fit are $E(\delta=0) = -0.777589(24)$, $A = 1.48(17)$, and $\gamma = 1.29(3)$ and give a reduced chi square of 1.58. This data agrees quite well with that of Black and Emery⁵⁶ who observed $\gamma=4/3$ in the 1D Heisenberg model. The energy of the symmetric lattice is within error bars of the exact thermodynamic limit of -0.77762 . The divergence of the lattice's susceptibility to bond ordering can be observed in Fig. 2; as the level of distortion approaches zero the bond order approaches the origin with infinite slope.

V. RESULTS FOR IONIC HUBBARD MODEL

The unit cell for the ionic Hubbard model is composed of two sites and the Hamiltonian is given in Eq. (1). In order to understand the meaning of the polarization and bond order in this system, it is helpful to consider first the noninteracting case with $U=0$, where one can visualize the electronic properties in terms of Wannier functions. At zero dimerization ($\delta=0$) the Wannier functions are centered on the sites whose energy is shifted by $+\Delta$ and $-\Delta$. Two electrons of opposite spin occupy the lowest energy Wannier function centered on the lower energy site in each unit cell. In the dimerized lattice ($\delta \neq 0$), the symmetry is broken and the centers of the Wannier functions are displaced from the sites creating a polarization. As U increases the electrons find it energetically undesirable to occupy the same site, and in the dimerized state the center of the distribution shifts further away from the low energy site. The limit of this displacement (i.e., polarization) is $P=1/2$ since one would never favor having more than one electron on the higher energy site. Similarly, the limit of the bond order is $B=2$ corresponding to isolated dimers.

As $\delta \rightarrow 0$ there are only three possibilities. If there is a spontaneous breaking of the inversion symmetry the polarization can assume any fractional value between 0 and 1/2. If there is no breaking of symmetry, there are still two possibilities since there are two centers of symmetry: the polarization can be 0 or 1/2. If the reference point defined to be zero is the usual band insulator where both electrons occupy the Wannier function centered on the lower energy site, it has been proposed^{13,57,58} that $P=1/2$ corresponds to a Mott insulator with no long range order.

We first report results of our study of the ionic Hubbard model with parameters fixed at the values used in previous work,^{13,57,58} so that direct comparisons can be made. The energy scale is set by defining $t_0=1$, $\Delta/t_0=0.5714$, and $\alpha t_0=40/7$. The previous conclusions with which we will compare are based upon exact diagonalization of the many-body Hamiltonian in small supercells^{13,58} and Hartree-Fock calculations.⁵⁷ The study¹³ using exact diagonalization of 8 site lattices with twisted boundary conditions found a jump of 1/2 in the electronic polarization for $\delta=0$, i.e., an electron in each unit cell being transported 1/2 lattice constant, at a critical value of U ($U_c=2.26$). This was interpreted as a transition between BI and MI phases, which was supported by Hartree Fock (HF) calculations that showed similar behavior at $U_c=2.46$. Extrapolations using larger cells of 12 sites⁵⁸ find $U_c=2.86$, presumably a more converged value. The key points are (i) the transition point U_c is found to be a metallic point with divergent delocalization, (ii) effective charges diverge and change sign at the transition, and (iii) there is no sign of the bond-ordered state predicted by Fabrizio *et al.*²⁵ This new state would have long range order and break the inversion symmetry of the lattice, thus allowing the polarization to take any fractional value.

The present work is based upon the QMC algorithms described earlier and the formulas for polarization and localization in Sec. III. The first step in applying the QMC methods is to find a trial wavefunction that has as much overlap with the true ground state as possible. This is achieved by optimizing the parameters $\{g, \Delta', \delta'\}$ to minimize the energy. To determine the optimal value of g we have used a newly devised technique that significantly reduces the amount of computational effort required.⁵⁹ Using the optimal Gutzwiller parameter the energy of $\Psi_T(g, \Delta', \delta')$ for different Δ' and δ' is sampled using VMC. We adjust Δ' and δ' to lower the VMC energy and measure it at several points in the neighborhood of its minimum. A curve fit is then performed using these points to determine the optimal Δ' and δ' . [Except where indicated all results for polarization, bond order and localization are determined by forward walking. This is not needed for some cases where the same results can be obtained using Eq. (21), but is essential in other cases.] The number of configurations over which expectation values are made varies with (i) the number of electrons and (ii) the proximity in the phase space defined by (U, Δ) to a critical point. On average for a lattice of 100 electrons we have sampled between 1–10 million statistically independent configurations in many-body space. Near critical points the correlation between measurements of the local form of an operator increases. This necessitates running the simulations

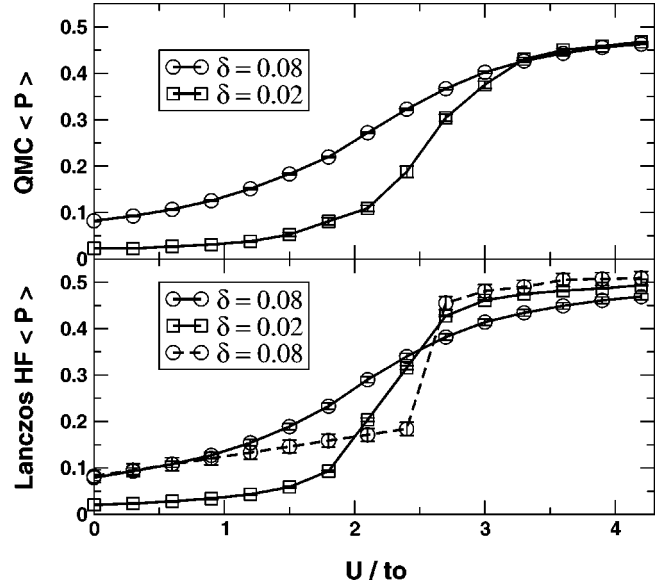


FIG. 3. QMC measurements of polarization (upper figure) extrapolated to large sizes compared to previous exact diagonalization and HF results (lower figure). Results are illustrated for staggered transfer integrals $t_i=t_0(1 \pm 0.02)$ (squares) and $t_i=t_0(1 \pm 0.08)$ (circles). The HF results are depicted by the dashed line in the lower figure.

longer so as to obtain unbiased estimates of the statistical error in our measurements.

A. Comparison with exact diagonalization and Hartree-Fock

Figure 3 shows the comparison of our results for the polarization P with those of the previous calculations of Refs. 13 and 57 for finite values of the distortion ($\delta=0.08$ and $\delta=0.02$). The present results are for periodic boundary conditions and extrapolated to the thermodynamic limit in $1/L$ as described in the following section. The results of Ref. 13 were obtained with 8 site rings and integrating over twisted boundary conditions. (The jump in P found in HF calculations for nonzero δ is an unphysical consequence of the mean field approximation that leads to an antiferromagnetic ground state that cannot occur in 1D.) The previous exact diagonalization results¹³ agree well with those of QMC for $\delta=0.08$. This is in agreement with previous studies using exact diagonalization^{36,55} on the usual Hubbard model which found that small cells of this size were sufficient to reach thermodynamic convergence in the $0.05 \leq \delta \leq 0.1$ regime, whereas convergence with cell size is worse for smaller δ .

The critical difference of our results from the previous exact diagonalization calculations¹³ is illustrated by the behavior as the magnitude of the distortion decreases to $\delta=0.02$. As shown in the lower panel the two curves for polarization P vs U cross. This is the basic result of Ref. 13: the crossing indicates that the effective charge Z^* , which is a derivative of the polarization with respect to lattice distortion ($Z^*=dP/d\delta$) changes sign. This indicates an anomalous reversal of the roles of the anion and cation, and in the limit of $\delta \rightarrow 0$ leads to $Z^* \rightarrow \infty$ and a discontinuous jump in polarization P at a critical value $U=U_c$. In contrast, no such behav-

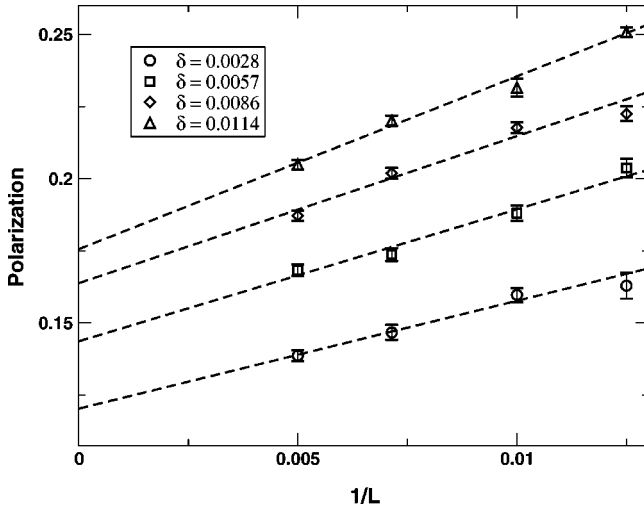


FIG. 4. The points represent the QMC P obtained using forward walking for system sizes of 80, 100, 140, and 200 sites for different levels of dimerization $\delta = \{0.0028, 0.0056, 0.0085, 0.0114\}$ in ascending order.

ior occurs in the present calculations: our results indicate that the effective charge $Z^* = dP/d\delta$ increases as $\delta \rightarrow 0$ but that it never changes sign. We attribute this difference to the fact that the correlation lengths increase near the transition point where $Z^* \rightarrow \infty$ so that the previous calculations on small cells are not sufficient. Even though the method of integrating over boundary conditions used in Refs. 13 and 57 allows one to use smaller cells than is required with periodic conditions, nevertheless, the size of the cell must exceed the correlation length. If it is smaller than the correlation length then artificial correlations are introduced that *maximize* the error.¹⁵ Indeed, it is agreed¹² that the localization length diverges, and a key point of the present work is that we are able to use cells of sufficient size to more correctly determine the behavior near the transition point.

B. Phase transition to bond-ordered (BO) state

We have measured the forward walking estimators for P , B , and $\langle \Delta^2 X \rangle$ and taken the limit of $\delta \rightarrow 0$ to study the nature of the quantum phase transition. The formulas used to obtain expectation values for polarization and localization are only accurate in the limit $L \rightarrow \infty$. This limit is taken by fitting measurements at finite L to a linear least squares fit in $(1/L)^\gamma$ and extrapolating to 0. We have found $\gamma=1$ to accurately account for the finite size effects of P and $\gamma=2$ for $\langle \Delta^2 X \rangle$. This scaling has only been found appropriate upon increasing the supercell size above a critical threshold which depends on the proximity of the metallic state. The accuracy of the finite size corrections to P are illustrated in Fig. 4 at $U = 2.7$ for different magnitudes of δ . The data in Fig. 4 was collected near the critical point of the phase transition, where size effects are large and must be treated accurately. If the system is sufficiently far from such a critical point, size effects are less pronounced, and there is a more rapid convergence to the thermodynamic limit.

Using the infinite L estimates for the polarization and localization on lattices dimerized by $\delta = \{0.0028, 0.0056,$

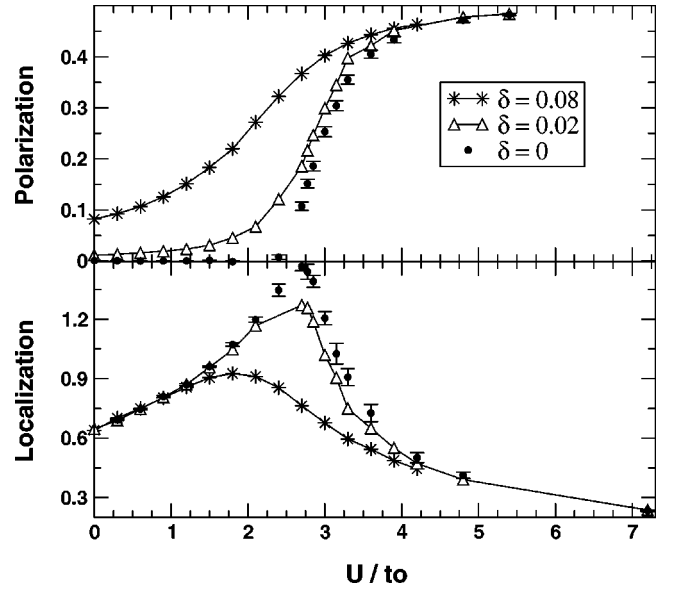


FIG. 5. $P(L=\infty)$ and $\langle \Delta^2 X \rangle$ for various levels of dimerization (δ). The extrapolated centrosymmetric polarization and localization is represented by the points with error bars.

$0.0085, 0.0114\}$ we have performed a linear least squares fit and extrapolated to the centrosymmetric limit ($\delta=0$). This method makes the assumption that the response of the lattice to dimerization is linear. However, near the phase transition nonlinearity will cause this to break down. In Fig. 5 we have plotted the polarization and localization of the ionic model for different magnitudes of dimerization.

The phase transition we find using QMC differs from the topological transition found using exact diagonalization and HF. As previously mentioned, in the BI and MI phases the polarization is restricted to 0 or 1/2. Resta and Sorella identified the shift from 0 to 1/2 as the signature of a BI \rightarrow MI transition. However, we find that P takes a continuous range of values in the centrosymmetric limit which can only occur only if the global inversion symmetry of the lattice is broken by a long range bond ordered (BO) state. Such a broken symmetry BO state was predicted by Fabrizio *et al.*²⁵ on the basis of field theory arguments in which he mapped the Hamiltonian onto two Ising spin models. The order parameter of this phase transition is the average bond order B given in Eq. (6). In Fig. 6 is given the spontaneous bond order B for the centrosymmetric lattice obtained by extrapolating to $\delta=0$ using the same values of δ as in Fig. 5. Here we fixed the supercell size to 142 sites and found the consequent size effects are within order of the error estimate for B .

We have attempted to classify the quantum phase transition by fitting the polarization and bond order of the centrosymmetric lattice to a function of the form

$$A[U - U_c]^\xi, \quad (26)$$

where ξ is the critical exponent and determines the universality class of the transition. A nonlinear least squares routine was used to fit the data, with fitted parameters U_c , A , and ξ listed in Table I. In Fig. 7 the data for P and B and the corresponding fits are plotted. Both quantities behave simi-

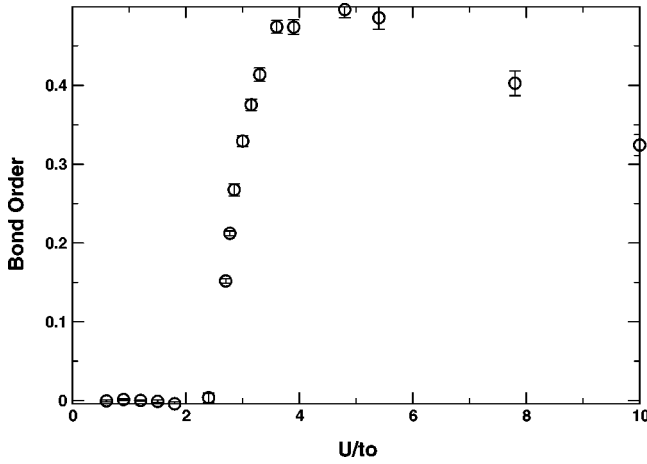


FIG. 6. QMC bond order of centrosymmetric lattice for $\Delta/t_0 = 0.5714$ and $L = 142$. Results obtained by extrapolating bond order on distorted lattices of $\delta = \{0.0028, 0.0056, 0.0085, 0.0114\}$ to $\delta = 0$.

larly near the critical point and the U_c of each is nearly identical. We find ξ for P and B are near $1/2$, the expected mean field exponent. On the other hand, Fabrizio *et al.*²⁵ predicted that the transition is of the Ising universality class and thus ξ should be $1/8$. We do not know whether the difference is real or it is simply due to the possibility that the range of $U - U_c$ over which the scaling belongs to the universality class is too small for us to observe in the present work.

Alternatively, the existence of the BO state can be observed by directly studying the symmetric lattice without any lattice distortion. Quantum phase transitions (QPT) are characterized by a symmetry breaking that occurs in the thermodynamic limit. Below U_c the lattice is a band insulator with no bond order but above U_c the electrons will spontaneously choose to bond order with $|B| \neq 0$. There are two such states characterized by the same magnitude but opposite sign of the bond order. For any finite system the ground state remains a linear combination of both. However, in the limit $L \rightarrow \infty$ one of these is arbitrarily chosen as the ground state. Even though the QMC simulations of the symmetric lattice for $U > U_c$ measure zero bond order and polarization for long-simulations, the imaginary time evolution of the simulations clearly depicts the projected ground state moving from one of these bond ordered states to the other. This phase separation gives rise to large autocorrelation times. The evolution of the bond order and polarization in imaginary time are illustrated in Fig. 8 for $U = 3.45$ and $L = 60$ sites. As the ground state moves between BO states of opposite symmetry both the polarization and dimerization are observed to

TABLE I. Fitting parameters for polarization and bond order. The quantities in parenthesis are the error in the last decimal place.

	A	U_c	ξ
P	0.44(1)	2.60(5)	0.60(10)
\hat{B}	0.49(1)	2.65(2)	0.39(4)

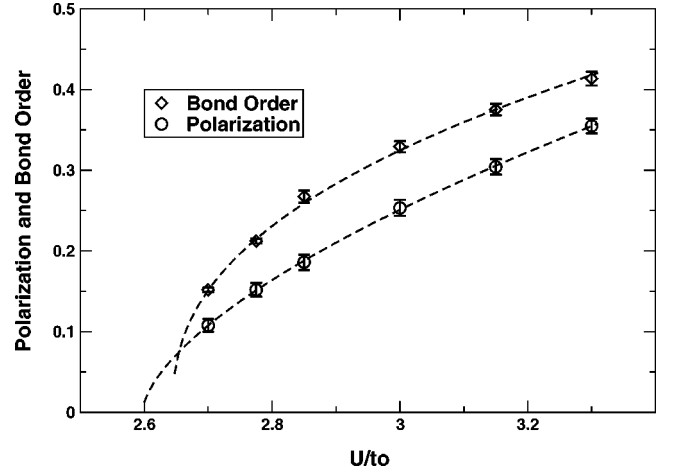


FIG. 7. Extrapolated polarization and bond order for the centrosymmetric ($\delta=0$) lattice near the critical point and their fits to Eq. (26).

change sign. This provides an alternative method of detecting the existence of the BO state.

At large U one might expect that there is a second transition to a symmetric Mott Insulator. Indeed, Fabrizio *et al.*²⁵ predict the existence of a Kosterlitz-Thouless transition for large U/Δ at which the bond order vanishes and the polarization is exactly $1/2$. However, we do not observe such a transition for any U considered which included values up to $U = 10$. The bond order does diminish but appears to asymptotically approach 0 and the polarization appears to converge to $1/2$ only in the limit of $U \rightarrow \infty$. It should be pointed out that working with such strongly correlated systems has the disadvantages that (i) fluctuations of the local estimators increase due to greater inaccuracies in the trial wavefunction and (ii) forward walking works so long as the trial wave

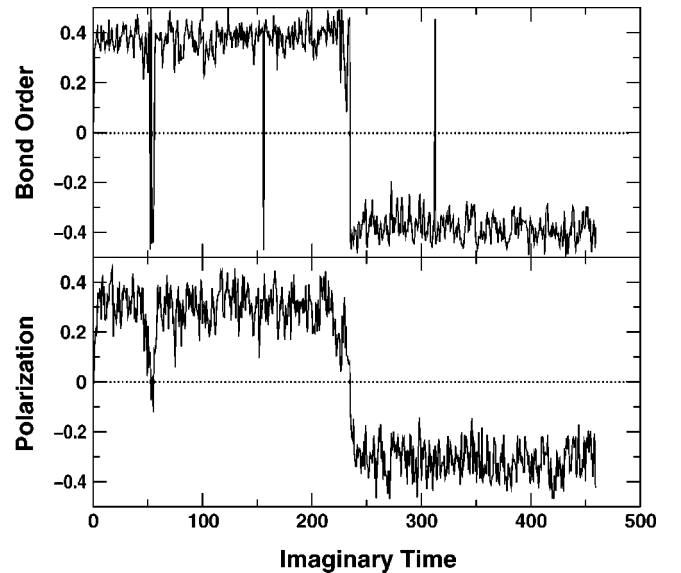


FIG. 8. Illustration of the phase separation in the symmetric case ($\delta=0$, $\Delta=0.5714$, $U=3.45$, and size $L=60$ sites) of the polarization and bond order. The lines depict the measurements over which averages are obtained in QMC.

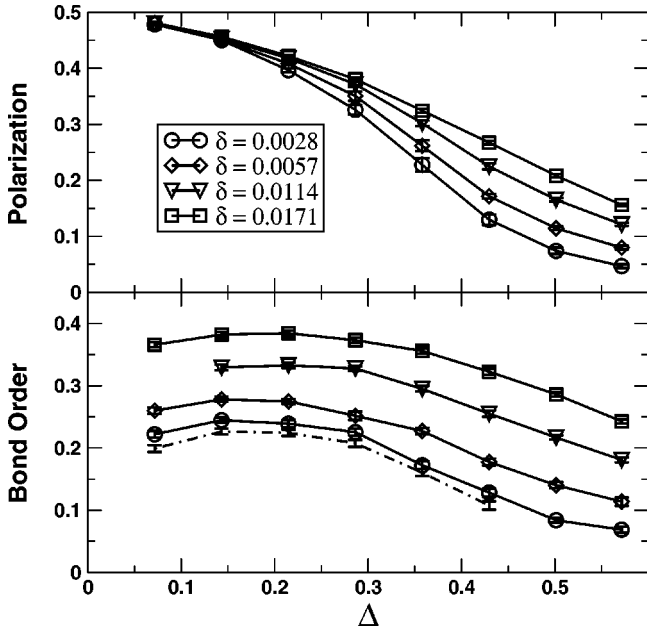


FIG. 9. Polarization and bond order vs ionic potential Δ for $\delta = \{0.0028, 0.0057, 0.0114, 0.0171\}$ and $U = 2.4$. The extrapolated bond order of the centrosymmetric lattice is denoted by the dotted line.

function has some overlap with the exact ground state and as U increases overlap with the exact ground state diminishes.

C. Phase transition as a function of ionicity Δ

An alternative approach to study the phase transition(s) is to diminish the ionic potential Δ while keeping U fixed, so that the ratio U/Δ increases. We have fixed the strength of electron correlation to $U = 2.4$ and studied the bond order and polarization for $0 < \Delta \leq 0.5714$. The behavior of the centrosymmetric lattice is inferred using two approaches (i) extrapolating results obtained on lattices with $\delta \neq 0$ and (ii) looking for evidence of phase separation in the symmetric case. Figure 9 shows the results of the first approach for a fixed supercell length of 142 sites. In the first we have neglected size effects and fixed the supercell length to 142 sites. At large Δ the single body contribution to the Hamiltonian is the dominant term and the lattice is a band insulator. Consequently the bond order and polarization are 0. However, as $\Delta \rightarrow 0$ a transition occurs to a BO state where the bond order is nonzero and the polarization assumes values between 0 and 1/2 as before. (The transition is rounded at this fixed cell length.) The bond order in the $\delta \rightarrow 0$ limit is shown by the dotted line in Fig. 9. These results were obtained by linearly extrapolating the bond order at finite δ . (No extrapolation was performed for the polarization since it is sensitive to size effects that were addressed in the previous section.)

Our results indicate the bond-order state exists at all values of $\Delta \neq 0$ studied. The finite value of the bond order for $\delta \rightarrow 0$ shown in Fig. 9 contrasts sharply with the vanishing of the bond order as $\delta \rightarrow 0$ for the nonionic Hubbard model ($\Delta = 0$) as shown in Fig. 2. At $\Delta = \delta = 0$, we always find

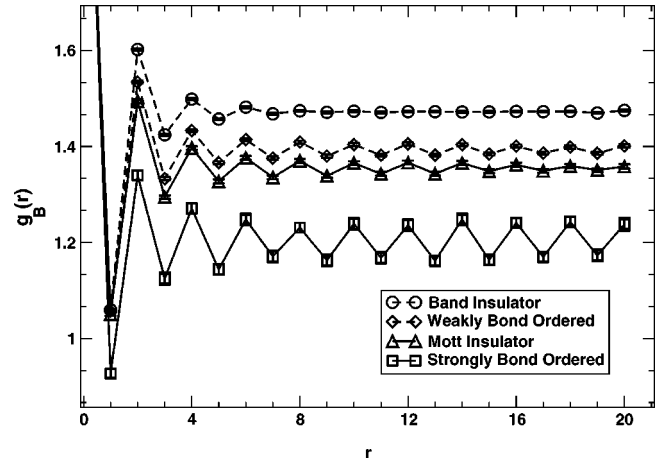


FIG. 10. Bond order correlation functions for the symmetric lattice ($\delta = 0$) for the (i) band insulating, (ii) weakly bond ordered (iii) Mott insulating, and (iv) strongly bond ordered regimes. The specific parameters are (i) $\Delta = 0.5714$, $U = 1.2$, $L = 60$, (ii) $\Delta = 0.1432$, $U = 2.4$, $L = 122$, (iii) $\Delta = 0$, $U = 2.5$, $L = 122$, and (iv) $\Delta = 0.5714$, $U = 3.45$, $L = 60$.

$B = 0$ and polarization equal 1/2 as they must be for a MI state with no long range order. However, our QMC simulations of the symmetric case ($\delta = 0$ and $U = 2.4$) at the smallest value of the ionic potential studied $\Delta = 0.0716$ reveal two BO states phase separating in imaginary time qualitatively the same as shown in Fig. 9. Thus from our studies, there is no sign of a second transition to a MI state as proposed by Fabrizio *et al.*²⁵ and the long range bond ordered state in Fig. 10 appears to exist for any finite $\Delta \neq 0$.

Our results imply that the MI state in 1D exists only within the usual Hubbard model and in ionic Hubbard lattices only in the limit $U = \infty$. At large U the usual Hubbard model has been mapped onto the Heisenberg spin model. The present finding suggests that such a mapping may be insufficient for ionic Hubbard models and that terms ignored or considered small possibly play a fundamental role.

D. Bond order correlation function and long range order

It is interesting to study the bond-order correlation function which reveals both the form of the short range order and the existence (or absence) of long range order. We define the bond order correlation function [$g_B(r)$] as

$$g_B(r) = \frac{1}{L} \left\langle \sum_i \hat{B}_i \hat{B}_{i+r} \right\rangle, \quad (27)$$

where \hat{B}_i is defined in Eq. (5) and is the strength of the i th bond of the lattice. Correlations of strong and weak bonds stagger this correlation function and are a signature of a bond ordered state. If we define $\Delta g_B(r) = [g_B(r) - g_B(r+1)](-1)^r$, it is straightforward to show that

$$\sqrt{2} \Delta g_B(r) \equiv B(r) \xrightarrow{r \gg r_{\text{corr}}} B, \quad (28)$$

where r_{corr} is a correlation length and B is the average bond order.

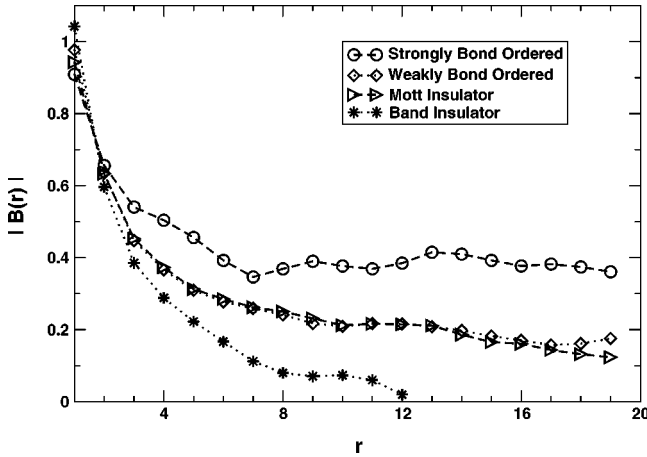


FIG. 11. Bond correlation $B(r)$ vs r [see Eq. (28)] for (i) band insulating, (ii) weakly bond ordered, (iii) Mott insulating, and (iv) strongly bond ordered regimes. The specific parameters are (i) $\Delta = 0.5714$, $U = 1.2$, $L = 60$, (ii) $\Delta = 0.1432$, $U = 2.4$, $L = 122$, (iii) $\Delta = 0$, $U = 2.5$, $L = 122$, and (iv) $\Delta = 0.5714$, $U = 3.45$, $L = 60$.

In Fig. 10 $g_B(r)$ is plotted for four separate cases, all with a symmetric Hamiltonian ($\delta = 0$): (i) $\Delta = 0.5714$, $U = 1.2$, $L = 60$; (ii) $\Delta = 0.1432$, $U = 2.4$, $L = 122$; (iii) $\Delta = 0$, $U = 2.5$, $L = 122$; and (iv) $\Delta = 0.5714$, $U = 3.45$, $L = 60$. The first case corresponds to the band insulating regime in which $g_B(r)$ exponentially approaches a constant, confirming the lack of any long range ordered phase. Conversely in the last case, which corresponds to the system in Fig. 8 that exhibited phase separation, it is clearly visible that $g_B(r)$ is staggered, signifying the presence of a long range bond ordered (BO) state. Finite size effects in each of these cases were determined to be minuscule and small systems were deemed sufficient to measure $g_B(r)$. The second case corresponds to diminishing Δ so as to move the system towards the established Mott State of the usual Hubbard model. At this point in the phase diagram the wells of the bimodal distribution are weakly defined; thus making it extremely difficult to observe the phase separation of the bond order parameter directly. In contrast, the bond order correlation function is clearly staggered, though to a lesser degree than that of the later case. Case (iii) is the Mott state of the usual Hubbard model. The staggered behavior of $g_B(r)$ does not approach a finite limit at large r , but rather tends to 0 in a fashion that appears to be a power law, contrary to the exponential convergence observed in the BI regime. Comparison of cases (ii) and (iii) shows that in each case the difference of $g_B(r)$ from its long range limit extends further than in the band insulating and strongly bond ordered cases. This shows that the fluctuations in the bond order are long ranged and leads to difficulties in the numerical calculations as the ionic potential tends to zero.

This estimate is exact when $r \gg r_{\text{corr}}$ where r_{corr} is the correlation length. Figure 11 shows $\langle \hat{B} \rangle(r)$ plotted vs r for the same cases as in Fig. 11. The band insulating estimate rapidly approaches 0 as a function of r . The strongly bond ordered system converges to an estimate of the bond order that is remarkably close to that obtained by extrapolating

from distorted lattices (0.45). The weakly bond ordered case appears to converge to a value near 0.18 which is in reasonable agreement with the extrapolated value of 0.2263(46). However, the $\langle \hat{B} \rangle(r)$ of the Mott insulator with $\Delta \equiv 0$ and the weakly bond ordered case with $\Delta \neq 0$ differ very little. No conclusion can be drawn as to whether or not a Mott state exists at small Δ . On the other hand, Figs. 10 and 11 clearly depict a bond ordered state for ionic lattices where Δ is of sufficient magnitude. As the ionicity is lowered, we do not know whether $g_B(r)$ decays according to a power law or it approaches a constant. The long ranged decay of $g_B(r)$ reflects the absence of a gap in the spectrum and exemplifies the unstable nature of the Mott State and its tendency to bond ordering. Only highly accurate measurements of the bond order correlation function for $r \gg r_{\text{corr}}$ can determine whether this instability to bond ordering exists at minuscule Δ .

VI. DISCUSSION

One of the primary results of the present work is the quantitative demonstration of the stability of the bond-ordered phase for interaction U above a critical value $U_c(\Delta)$ for any nonzero Δ . Most of our work was carried out through dimerizing the lattice by δ and examining the $\delta \rightarrow 0$ limit. There were two reasons for this (i) this is an aid in the actual calculations which are stabilized by the applied bias and (ii) the variation with dimerization δ is important in and of itself. Regarding the second point, it is well known that the ordinary nonionic Hubbard model is unstable to dimerization, with a logarithmic Peierls instability at $U = 0$ that becomes a stronger fractional power law instability at large U .^{35–37,33,55,56} Our work shows that as a function of U/Δ the ionic Hubbard model undergoes a phase transition from a stable nondimerized BI phase to a correlated phase in which the instability is *more severe* than in the nonionic Hubbard model. This is evident in comparison of Fig. 2 with Figs. 5 and 7. In the nonionic case (Fig. 2), the decrease of the bond order with δ is clearly observed and is consistent with previous theoretical predictions of the power law form. However, in all the calculations for the ionic model for U/Δ above the critical value, the average bond order $\langle \hat{B} \rangle$ is found to extrapolate to a nonzero value. This is observed even for δ much smaller than previous studies. From this evidence alone there are two possibilities: (1) the BO phase with broken symmetry is stable at zero dimerization or (2) there is nonanalytic behavior as $\delta \rightarrow 0$ which is even stronger than that for the nonionic Hubbard model.

This result is sufficient to draw conclusions about real 1D systems in which the sites are allowed to dimerize if this leads to lower energy. In either of the two scenarios described above, dimerization would always occur (except in the BI phase). In the first scenario the BO phase would occur spontaneously and by symmetry there would always be an accompanying lattice distortion. In the second scenario, dimerization would occur due to the nonanalytic energy vs δ which would lead to bond order. The symmetric Mott insulator would never occur and the only transition would be

from a BI phase to a dimerized BO phase. This is in agreement with previous results that electronic correlation enhances the instability to bond ordering.^{35–37,33,55,56}

At this point we can compare with experiment on 1D materials. Experimental works by Torrance *et al.*⁶⁰ observed a second order transitions between neutral (BI) and ionic (BO) states in organic charge transfer solids. The transition occurs upon applying pressure over a wide range of temperatures and was attributed to the rise in Madelung energy of the crystal. No state synonymous to the Mott state was observed.

Among the interesting consequences of the stability of the BO state is the existence of fractional charges.^{61,25} For the case of a dimerized or bond-ordered state, the charge is an irrational fraction the value of which depends upon the value of Δ .^{61,25}

Other work on related systems also has identified BO phases. Recent work by Nakamura²⁶ in the extended Hubbard model has found a rich phase diagram in which there are two transitions from a BI→BO and BO→MI regime. The extended Hubbard model differs from the ionic model studied here in that there is an additional next nearest neighbor coulomb potential V and no ionic potential Δ . Nakamura identifies the first transition as belonging to the Gaussian universality class and the later as a Kosterlitz-Thouless transition. The BO phase observed by Nakamura exists at all V down to the usual Hubbard model ($V=0$); where both the Gaussian and the KT transitions coexist. We can imagine the U_c at which the BI→BO transition takes place increasing concurrently as the ionic potential is increased from zero.

Let us now consider why the BO phase was not found in previous studies that used exact-diagonalization Lanczos techniques to treat small finite systems.^{13,57} If the BO state is the ground state then, of course, it is degenerate and one can form linear combination of the states

$$\Psi_0 = \cos(\theta)\Psi_+ + \sin(\theta)\Psi_-, \quad (29)$$

each of which has no net bond order. For finite systems existence of the BO state can be inferred from correlation functions; however, to our knowledge this has not been done in other work. A second reason that the BO states have not been observed may be that there is no bimodal distribution for the small cells studied by exact diagonalization. We have addressed this issue by using QMC to determine average bond order on distorted lattices of $14 \leq L \leq 62$ sites and extrapolating to the centrosymmetric limit. At a point in the phase diagram ($\Delta=0.0716$, $U=2.4$) where the correlation lengths are large, we find that lattices with less than 50 sites do not exhibit the BO phase; only for larger supercells do we find the phase separation of the two BO states. As we have pointed out, this is the key difference in our approaches: if we want to determine the behavior near the critical point, we expect to need large cells for which exact diagonalization methods are not currently feasible.

Recent work using the density matrix renormalization group (DMRG) method has reported results for charge Δ_c and spin Δ_s gaps in these models. This approach should enable one to distinguish the phases since (i) $\Delta_c = \Delta_s \neq 0$ in the BI phase, (ii) $\Delta_c \neq \Delta_s \neq 0$ in the BO phase, and (iii) $\Delta_c \neq 0$

but $\Delta_s = 0$ in the MI phase. It was found to be very difficult and to require extremely large cells to determine spin gaps in the BO/MI phases, and the two reports came to opposite conclusions on the existence of the BO phase.

In our QMC calculations we have also determined the charge and spin gaps. Our estimates of the charge gap are in qualitative agreement with other works; however, the spin gap is very small in all cases except in the BI regime and statistical noise does not permit an accurate determination of such small gaps in QMC.

Both DMRG calculations find the spin gap to vanish, i.e., the MI phase to be the ground state for large U . We have no direct explanation of this difference: it may be that our procedure is not sufficiently accurate to determine the BO-MI transition, which is the most difficult part of the present work. On the other hand, it may be that the DMRG calculations on finite cells with open boundary conditions may have difficulties: the surface effects break the symmetry of the problem which may lead to extremely problematic size effects and potential errors. The BO-MI transition was predicted using a weak-coupling effective field theory and the charge gap of the Plain Hubbard model.²⁵ It is possible that at large U this theory is not applicable and cannot accurately predict whether the MI state actually exists. In any case, we are very confident that our work establishes that the BO state is either the ground state or very close to the ground state in energy; this is clear from our tests on the ordinary Hubbard model shown in Fig. 1.

VII. CONCLUSIONS

We have studied the phase diagram of an idealized dielectric, the 1D ionic Hubbard model proposed by Nagosa²³ and Egami.²⁴ This model undergoes a phase transition as a function of the on-site interaction U , which has been a source of controversy. The only previous quantitative studies^{13,57} concluded that at a critical U_c there is an abrupt ‘‘topological’’ transition from a band insulator to a Mott insulator with no broken symmetry or long range order in either phase. The signature of the transition was found to be an abrupt change of 1/2 in the polarization at which the effective charge diverged signifying the delocalization of the electron states.^{13,57} Recently, however, there has been a prediction²⁵ that this model would exhibit two quantum phase transitions: the first signifying a change of state from a band insulator to a broken symmetry phase with long range alternating bond order, and the second a transition to the Mott insulator.

We have studied this model using quantum Monte Carlo methods which allow the simulation of much larger systems than studied by exact diagonalization.^{13,57} To our knowledge, this is the first application of QMC to determine both the polarization and localization of an electronic system. For this model our QMC methods are in principle exact, since there is no sign problem, so long as our trial function has nonzero overlap with the true ground state. We evaluate the expectation values of the bondorder, polarization, and localization using the expressions Eqs. (5), (9), and (10). It is found that upon crossing a critical value U_c a change of phase occurs from a band insulating to bond-ordered state. The bond order

develops continuously (see Fig. 8) as a function of $U - U_c$ and since the inversion symmetry is broken, the polarization also varies continuously, unlike the results of the small cell exact-diagonalization calculations.¹³ The existence of bond order is also demonstrated in the QMC simulations by the “flip-flop” between left and right BO states.

The critical behavior is uniquely determined by fitting the bond order and polarization to a scaling function near the critical regime. We find an exponent near 1/2, which differs from that for the Ising class proposed in Ref. 25; however, it may be that we are outside of the regime in which the scaling belongs to the appropriate universality class. In addition, we found that there is a metallic point at U_c where the system is metallic. At this point the charge gap must vanish which we have found in pure ground state calculations by determining the fluctuations of the polarization. The calculations determine quantitatively the localization length,^{13–15} which diverges at the transition.

We have searched for the proposed transition to a Mott insulating state, but we have not observed such a transition from the bond ordered regime even for very large U or very small Δ . Even the smallest value of Δ considered in this study ($\Delta/t_0 = 1/14 \ll U/t_0 = 2.4$) is sufficient to cause the ionic Hubbard model to be unstable to bond ordering, although there is no broken symmetry in the usual Hubbard model ($\Delta \equiv 0$), neither in the exact solution²² nor in our results. Thus our results show that the instability to dimerization is even stronger in the ionic model than that known previously for the ordinary nonionic Hubbard

model.^{35–37,33,55,56} Furthermore, for the centrosymmetric lattice ($\delta=0$), calculations of correlation functions and observations of “flip-flop” between left and right bond-ordered states in the QMC simulations provides further evidence for the stability of the bond-ordered state.

Finally, these results imply that if dimerization is allowed (which is always the case in real materials since the atoms can always dimerize if it lowers the energy) then the symmetric Mott state is never stable and the only phase transition is from the symmetric BI to the dimerized BO state. This is experimentally confirmed by Torrance *et al.*⁶⁰, where upon increasing the electronic interaction a BI→BO transition takes place.

ACKNOWLEDGMENTS

We gratefully acknowledge Erik Koch for his help implementing lattice quantum Monte Carlo methods and David Campbell, Michele Fabrizio, Eduardo Fradkin, Erik Koch, Gerardo Ortiz, Rafaella Resta, Anders Sandvik, Pinaki Sengupta, Ivo Souza, and David Vanderbilt for invaluable discussions. This work would not have been feasible without the computational resources of the National Supercomputing Center at the University of Illinois and the Materials Research Laboratory. We are especially grateful to the NT supercluster, managed by Rob Pennington and Michael Showerman, which provided the majority of the computational resources for this study. This work was supported by the National Science Foundation Grant No. DMR 9802373.

-
- ¹M. Imada, A. Fujimori, and Y. Tokura, *Rev. Mod. Phys.* **70**, 1039 (1998), and references therein
- ²N.F. Mott, *Proc. R. Soc. London, Ser. A* **382**, 1 (1982).
- ³N.F. Mott, *Proc. Phys. Soc., London, Sect. A* **62**, 416 (1949).
- ⁴J.C. Slater, *Phys. Rev.* **82**, 538 (1951).
- ⁵D.H. Lee and R. Shankar, *Phys. Rev. Lett.* **65**, 1490 (1990).
- ⁶D. J. Griffiths, *Introduction to Electrodynamics* (Prentice-Hall, Englewood Cliffs, NJ, 1989).
- ⁷L.D. Landau, E.M. Lifshitz, *Electrodynamics of Continuous Media* (Pergamon Press, Oxford, England, 1988).
- ⁸W. Kohn, *Phys. Rev.* **133**, A171 (1964).
- ⁹R.D. King-Smith and D. Vanderbilt, *Phys. Rev. B* **47**, 1651 (1993).
- ¹⁰G. Ortiz and R.M. Martin, *Phys. Rev. B* **49**, 14 202 (1994).
- ¹¹R. Resta, *Phys. Rev. Lett.* **80**, 1800 (1998).
- ¹²R. Resta and S. Sorella, *Phys. Rev. Lett.* **82**, 370 (1999).
- ¹³R. Resta, S. Sorella, *Phys. Rev. Lett.* **74**, 4738 (1995).
- ¹⁴A.A. Aligia and G. Ortiz, *Phys. Rev. Lett.* **82**, 2560 (1999).
- ¹⁵I. Souza, T. Wilkens, and R.M. Martin, *Phys. Rev. B* **62**, 1666 (2000).
- ¹⁶M.V. Berry, *Proc. R. Soc. London, Ser. A* **392**, 45 (1984).
- ¹⁷C. Gros, *Z. Phys. B: Condens. Matter* **86**, 359 (1992).
- ¹⁸D.J. Scalapino, S.R. White, and S. Zhang, *Phys. Rev. B* **47**, 7995 (1993).
- ¹⁹N. Beyers and C.N. Yang, *Phys. Rev. Lett.* **7**, 46 (1961).
- ²⁰J. Hubbard, *Proc. R. Soc. London, Ser. A* **276**, 238 (1963).
- ²¹J.M.P. Carmelo *et al.*, *The Hubbard Model: It's Physics and Mathematical Physics* (Plenum Press, New York, 1995).
- ²²E.H. Lieb and F.Y. Wu, *Phys. Rev. Lett.* **25**, 1445 (1968).
- ²³N. Nagaosa and J. Takimoto, *J. Phys. Soc. Jpn.* **55**, 2735 (1986).
- ²⁴T. Egami, S. Ishihara, and M. Tachiki, *Science* **261**, 1307 (1993).
- ²⁵Michele Fabrizio, Alexander O. Gogolin, and Alexander A. Nersisyan, *Phys. Rev. Lett.* **83**, 2014 (1999).
- ²⁶Masaaki Nakamura, *Phys. Rev. B* **61**, 16 377 (2000).
- ²⁷E.V. Tsiper and A.L. Efros, *J. Phys.: Condens. Matter* **9**, L561 (1997).
- ²⁸Yasutami Takada and Manabu Kido, cond-mat/0001239 (unpublished).
- ²⁹S. Qin, J. Lou, T. Xiang, Z. Su, and G. Tian, cond-mat/0004162 (unpublished).
- ³⁰W. M. C. Foulkes, L. Mitás, R. J. Needs, and G. Rajagopal, (unpublished).
- ³¹Joel W. Cannon and Eduardo Fradkin, *Phys. Rev. B* **41**, 9435 (1990).
- ³²Nandini Trivedi and D.M. Ceperley, *Phys. Rev. B* **41**, 4552 (1990).
- ³³J.E. Hirsh, *Phys. Rev. Lett.* **51**, 296 (1983).
- ³⁴I.I. Ukrainskii, *Sov. Phys. JETP* **49**, 381 (1979).
- ³⁵D. Baeriswyl and K. Maki, *Phys. Rev. B* **31**, 6633 (1985).
- ³⁶G.W. Hayden and Z.G. Soos, *Phys. Rev. B* **38**, 6075 (1988).
- ³⁷P. Horsch, *Phys. Rev. B* **24**, 7351 (1981).
- ³⁸W.P. Su, J.R. Schrieffer, and A.J. Heeger, *Phys. Rev. Lett.* **42**, 1698 (1979).

- ³⁹Charles Kittel, *Introduction to Solid State Physics* (Wiley, New York, 1986).
- ⁴⁰C.A. Coulson, Proc. R. Soc. London, Ser. A **169**, 413 (1939).
- ⁴¹Eduardo Fradkin, *Field Theories of Condensed Matter Systems* (Addison-Wesley, New York, 1991).
- ⁴²R.M. Martin and G. Ortiz, Solid State Commun. **102**, 121 (1997).
- ⁴³L. Mihaly and Michael C. Martin, *Solid State Physics: Problems and Solutions* (Wiley, New York, 1996).
- ⁴⁴R. Resta, Rev. Mod. Phys. **66**, 899 (1994).
- ⁴⁵N. Marzari and D. Vanderbilt, Phys. Rev. B **56**, 12 847 (1997).
- ⁴⁶F. Bolton, Phys. Rev. B **54**, 4780 (1996).
- ⁴⁷G. Ortiz, D.M. Ceperley, and R.M. Martin, Phys. Rev. Lett. **71**, 2777 (1993).
- ⁴⁸B. L. Hammond *et al.*, *Monte Carlo Methods in Ab Initio Quantum Chemistry* (World Scientific, Singapore, 1994).
- ⁴⁹N. Metropolis, A.W. Rosenbluth, M.N. Rosenbluth, A.M. Teller, and E. Teller, J. Chem. Phys. **21**, 1087 (1953).
- ⁵⁰M.C. Gutzwiller, Phys. Rev. Lett. **10**, 159 (1963).
- ⁵¹Guozhong An and J.M.J. van Leeuwen, Phys. Rev. B **44**, 9410 (1991).
- ⁵²Steven E. Koonin, and Dawn C. Meredith, *Computational Physics* (Addison-Wesley, New York, 1990).
- ⁵³D.F.B. ten Haaf *et al.*, Phys. Rev. B **51**, 13 039 (1995).
- ⁵⁴K. Hashimoto, Int. J. Quantum Chem. **28**, 581 (1985).
- ⁵⁵Z.G. Soos, S. Kuwajima, and J.E. Mihalick, Phys. Rev. B **32**, 3124 (1985).
- ⁵⁶J.L. Black and V.J. Emery, Phys. Rev. B **23**, 429 (1981).
- ⁵⁷G. Ortiz, P. Ordejón, R.M. Martin, and G. Chiappe, Phys. Rev. B **54**, 13 515 (1996).
- ⁵⁸N. Gidopoulos, S. Sorella, and E. Tosatti, cond-mat/9905418 (unpublished).
- ⁵⁹Erik Koch, Olle Gunnarsson, and Richard M. Martin, Phys. Rev. B **59**, 15 632 (1999).
- ⁶⁰J.B. Torrance *et al.* Phys. Rev. Lett. **47**, 1747 (1981).
- ⁶¹M.J. Rice and E.J. Mele, Phys. Rev. Lett. **49**, 1455 (1982).